*Journal of Oceanography*, Vol. 61, pp. 539 to 548, 2005

# Significance of High-Frequency Wind Forcing in Modelling the Kuroshio

TAKUJI WASEDA[1]*, HUMIO MITSUDERA[2], BUNMEI TAGUCHI[3] and KUNIO KUTSUWADA[4]

[1]*Frontier Research System for Global Change and the International Pacific Research Center, University of Hawaii, HI 96822, U.S.A.*
[2]*Institute of Low Temperature Science, Hokkaido University, Sapporo 060-0819, Japan*
[3]*Department of Meteorology, University of Hawaii, HI 96822, U.S.A.*
[4]*School of Marine and Technology, Tokai University, Shizuoka 424-8610, Japan*

(Received 4 November 2003; in revised form 25 November 2004; accepted 25 November 2004)

**Motivated by an analysis of a satellite sea surface temperature image suggesting that a train of extra-tropical cyclones induces amplification of the Kuroshio meander, a regional Kuroshio/Oyashio general circulation model was used to investigate the impact of high-frequency wind on the Kuroshio path variations. Near Japan, the standard deviation of the wind stress curl can be 10 times larger than the monthly mean, so the synoptic variations of the wind stress curl cannot be neglected. With the bimodal Kuroshio case realized in the model, sensitivity tests were conducted using monthly and daily mean QuikSCAT-derived wind stress forcings. The comparison showed that the high-frequency local wind perturbed the Shikoku recirculation gyre (SRG) and caused a transition of the path from straight to meander. The strong anticyclonic eddy within the SRG triggered the meander in the latter case. The high-frequency wind perturbed the motion of the eddy that would have otherwise detached from the Kuroshio, migrated south and terminated the meandering state. The result reinforces the suggestion from previous studies that the anticyclonic eddy within the SRG plays an active role in controlling the Kuroshio path variations.**

Keywords:
· Kuroshio meander,
· Shikoku recirculation gyre,
· QuikSCAT.

## 1. Introduction

The Kuroshio has been extensively studied in the past not only because of its significance in transporting mass and heat but because of its unique dynamical feature south of Japan; the current takes two preferred paths, one straight and one meandering (Masuda, 1982; Kawabe, 1985). Early theoretical work based on stationary Rossby waves with topographic constraint on the eastern and the western ends suggested that the meander path occurs at low-volume transport and the straight path at high-volume transport (White and McCreary, 1976; Yasuda *et al*., 1985). However, later studies indicated otherwise, and it is now generally recognized that the low-volume transport results in a straight path while the high volume transport results in a meander path (Chao, 1984; Yasuda and Yoon, 1987; Akitomo *et al*., 1991). The theoretical work suggests that both straight and meander paths are possible at intermediate transports, and the transition between the paths occurs as a hysteresis when the transport changes. However, recent modelling studies suggest that the transition between straight and meander paths occurs even with relatively small change in the Kuroshio transport (Hurlburt *et al*., 1996; Akitomo *et al*., 1997; Qiu and Miao, 2000). It is known that the seasonal variation of the Kuroshio transport is much smaller than expected from the Sverdrup transport (Kagimoto and Yamagata, 1996; Imawaki *et al*., 2001a), and the observed interannual variation of the Kuroshio is relatively small, too (Kawabe, 1995; Imawaki *et al*., 2001b). These recent findings of relatively constant Kuroshio volume transport suggest that the Kuroshio's basic state is almost always bimodal.

The active role of an anticyclonic eddy within the Shikoku recirculation gyre (hereafter SRG) in causing the Kuroshio to transition between straight and meandering path states has been discussed recently on the basis of both observation and numerical experiments. Ebuchi and Hanawa (2000), Mitsudera *et al*. (2001), and Waseda *et al*. (2003), showed that a strong anticyclonic eddy exists

* Corresponding author. E-mail: waseda@naoe.t.u-tokyo .ac.jp
Present address: Department of Environmental and Ocean Engineering, University of Tokyo, Hongo, Bunkyo-ku, Tokyo 113-8656, Japan.

a)

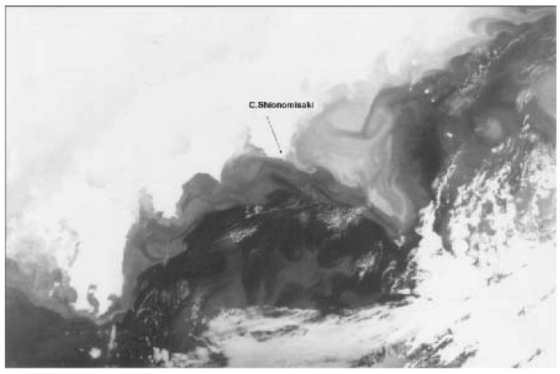


b)

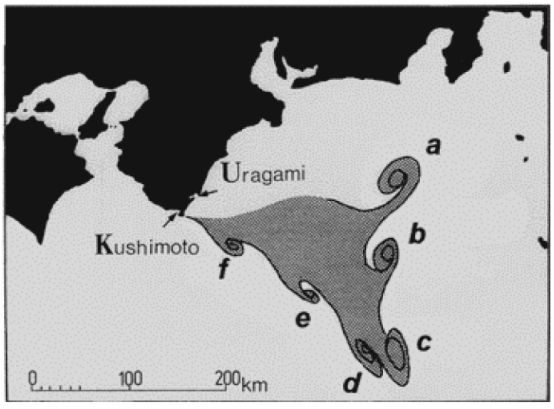


Fig. 1. a) AVHRR image showing shedding of cyclonic vorticities from the Kii peninsula; b) Schematic of the cyclonic eddy shedding from the Kii peninsula, Both are adopted from Nishimura (images obtained from http://www.rs.noda.tus.ac.jp/~kaiyou/eddy.htm).

within the SRG and actively interacts with the Kuroshio, causing its amplitude to oscillate as the eddy rotates within the SRG. As other studies have shown, this anticyclonic eddy originates from south and east of the SRG, suggesting that an external forcing can trigger the transition of the Kuroshio path (Akitomo *et al*., 1991; Endoh and Hibiya, 2001; Mitsudera *et al*., 2001; Waseda *et al*., 2002; Ebuchi and Hanawa, 2003). Throughout this paper, we view the Kuroshio system from a regional perspective where the inflow and outflow of the domain of interest are specified. "External" refers to perturbations that originate from outside the domain or from surface flux. Far less attention so far has been given to the possibility of the local wind as an external forcing, and we have conducted numerical experiments using satellite-derived high-frequency wind stress to investigate this possibility.

This study was originally motivated by an analysis of the AVHRR image by Nishimura (Fig. 1(a)) (Nishimura, 1998), who observed in April 1983 that a series of extra tropical cyclones passed through Japan and coincided with a sequence of cyclonic eddy shedding from the Kii peninsula inshore of the Kuroshio (Fig. 1(b)). Nishimura further suggests that these cyclonic eddies eventually merge as a result of inverse cascading, enlarging the cyclonic circulation inshore of the Kuroshio and, eventually, the Kuroshio meanders. He suggests that the eddy shedding was caused by resonance of the external atmospheric forcing and the ocean at about 5-day intervals. However, he did not show how the atmospheric forcing excited the flow shedding at the Kii peninsula.

Our previous study (Waseda *et al*., 2003) using a regional GCM suggested that the shedding of the cyclonic eddy at the Kii peninsula can be caused when the anticyclonic eddy within the SRG approaches the Kii peninsula (Fig. 2). When the anticyclonic eddy approaches the Kii

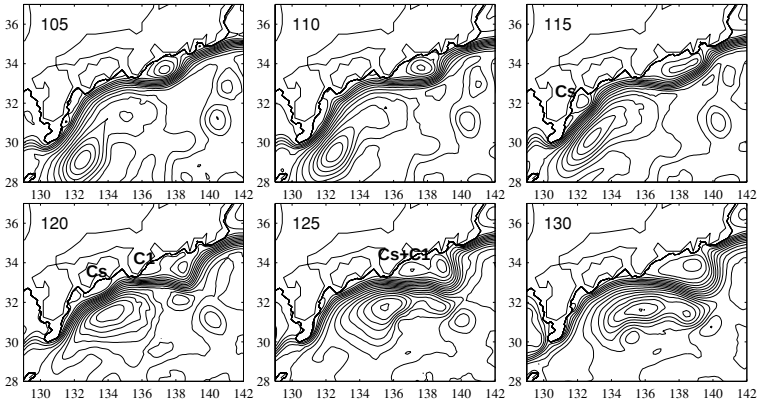


Fig. 2. Eddy shedding at the Kii peninsula from the numerical simulation. C1 and Cs represents cyclonic eddies that appear inshore the Kuroshio. Contours are sea surface elevation; c.i. 0.1 m.

peninsula, cyclonic eddies are shed inshore of the Kuroshio (eddy C1 is shed first at day 120 and eddy Cs is shed at day 125), and eventually merged (see Waseda *et al*. (2003) for detailed description). This result suggests that the shedding of the cyclonic eddies at the Kii peninsula may be a result of the interaction of the anticyclonic eddy in the SRG and the Kuroshio.

The objective of the current research is to investigate the impact of high-frequency, high-wavenumber wind stress forcing on the Kuroshio path at its bimodal state. Such impact has not been thoroughly investigated in the past despite recognition of strong wind stress variability in the vicinity of the Kuroshio south of Japan. Furthermore, because of the large subdiurnal variability of the wind system, the magnitude of the daily wind stress derived from the daily wind speed may not have been appropriate in the previous studies because of its nonlinearity. In the following sections we first describe the nature of the wind stress near Japan and compare QuikSCAT-derived wind stress, climatological wind stress and numerical weather prediction model wind stresses in Section 2. We then describe the numerical setting and present the experimental results using QuikSCAT-derived wind stress forcing in Section 3. The focus is on the role of the anticyclonic eddy within the SRG and how that is influenced by high-frequency wind forcing. The conclusion follows.

## 2. Wind Stress near Japan

We have compared different wind and stress products in the Kuroshio/Oyashio/Extension region (120°E–170°E, 25°N–55°N): the QuikSCAT-derived gridded wind and stress (J-OFURO, 1 × 1 degree, daily)*; the ECMWF operational wind and stress (~1.125 degree, daily)**; and the Hellerman-Rosenstein wind and stress. The annual mean wind stresses compare well with each other, as shown in the scatter digaram (Fig. 3). The wind speed histograms of the ECMWF operational wind and the QuikSCAT-derived wind during 2000 and 2001 were nearly identical (not shown). The means are therefore consistent among these products.

For the dynamics of the ocean, the variation of wind stress curl is the most significant measure of the high-frequency wind perturbation. Because of the variability associated with the passage of fronts and extra-tropical cyclones, the standard deviation of the wind stress curl is an order of magnitude larger than the mean (Fig. 4). Time variations of the curl would then have intermittent spikes riding on top of a slowly varying seasonal cycle which is an order of magnitude smaller than the spikes associated with synoptic events (Fig. 5). The peak value of the wind stress curl is on the order of $1.0 \times 10^{-6}$ kg m$^{-2}$s$^{-2}$ which is equivalent to about O($10^{-3}$) cm s$^{-1}$ Ekman pumping velocity, to about O(0.1) cm s$^{-1}$ in horizontal velocity if we consider the ratio of the horizontal and the vertical scales to be about 100. This is approximately 1/1000 of the maximum velocity of the Kuroshio current, and randomly perturbs the current assuming that the synoptic wind field is uncorrelated with the underlying ocean.

In addition to such synoptic scale (~days) variations, temporal changes shorter than the diurnal cycle due to the propagating gravity waves, deep convection, and boundary layer turbulence can be crucial factors in deriving wind stress from wind speed because of the nonlinearity of their relation. We now proceed to analyze the ECMWF product to investigate the significance of wind stress variations of less than a day. Typically, the wind stress is derived from the wind speed using a bulk formula

$$\tau = \rho C_D |U|^2 \tag{1}$$

where $C_D$ itself is a function of wind speed. Since both $C_D$ and $U$ have temporal variations shorter than the diurnal cycle, the daily averaged stress is larger than the stress derived from daily averaged wind speed

$$\langle \rho C_D |U|^2 \rangle > \rho C_D \langle |U| \rangle^2 \tag{2}$$

where < > represents a daily average. To evaluate the impact of the temporal variations of less than a day, we estimated the ratio of the left-hand-side term to the right-hand-side term of (2) as an indicator; $I \equiv \langle \rho C_D |U|^2 \rangle / \rho C_D \langle |U| \rangle^2$.

The analysis revealed that the daily averaged wind stress is about 25% larger than the wind stress derived from daily mean wind speed (Fig. 6). In this analysis we have used the drag coefficient suggested by Yelland and Taylor (1996) which is essentially the same as that of Large and Pond (1981) and is quite consistent with the ECMWF parameterization, as documented by Bonekamp *et al*. (2002); see their figure 9. The effective increase of wind stress by daily averaging is a rather surprising re-

*J-OFURO: Japanese Ocean Flux data sets with Use of Remote sensing Observations. The gridded wind-stress and wind vectors were obtained using QuikSCAT level 2 data and the bulk method based on Large and Pond (1981). The period covered is from July 1999 through 2001, the spatial resolution is 1.0 degree by 1.0 degree and the temporal resolution is daily. Details of the construction procedure are described in Kutsuwada (1998) and Kubota *et al*. (2002).

**Distributed as ECMWF TOGA Global Advanced Operational Surface Analysis and ECMWF TOGA Global Supplementary Fields respectively. Their description, as well as the evolution of the ECMWF forecasting system for the period 1985 to the current day can be obtained from the ECMWF web page (http://www.ecmwf.int/products/data/).

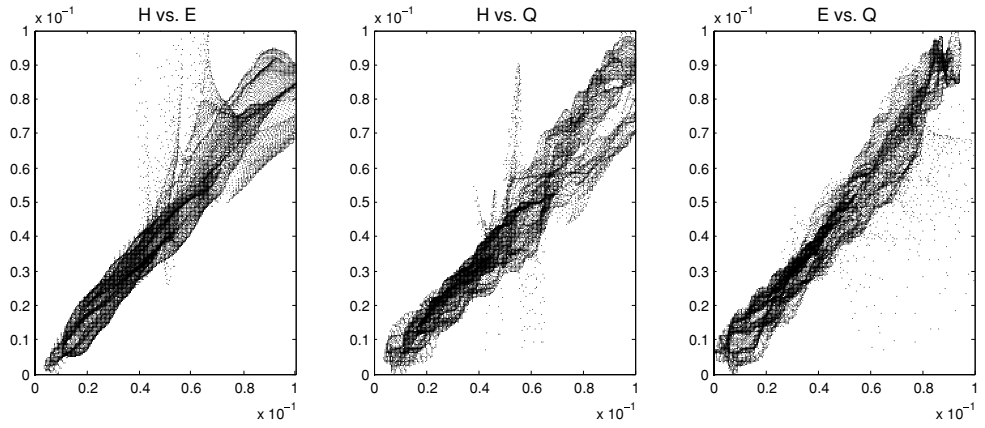


Fig. 3. Scatter diagram comparing mean wind stresses from Hellerman-Rosenstein (H), ECMWF operational wind (E) and QuikSCAT derived wind (Q). The units are N $m^{-2}$. Left: abscissa, H; ordinate E. Center: abscissa, H; ordinate Q. Right: abscissa, E; ordinate, Q.

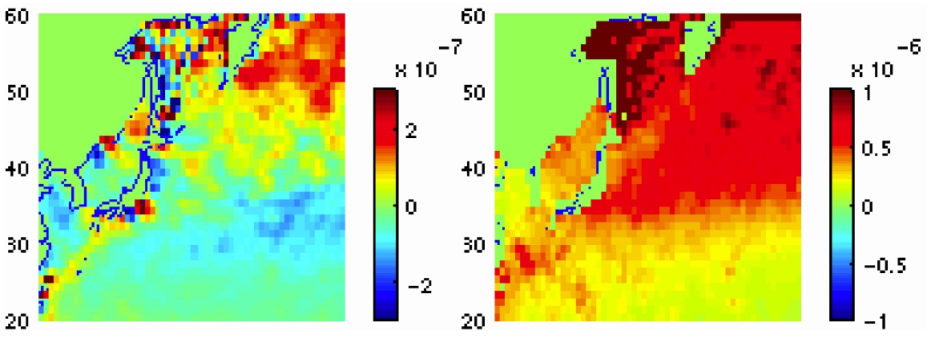


Fig. 4. Mean and the standard deviation of the wind stress curl in the Kuroshio, the Oyashio and the Extension regions. Right panel shows the standard deviation, which is an order of magnitude larger than the mean field shown in the left panel (note that the color scales are different; the unit is N $m^{-3}$).

sult since contribution from sub-diurnal variation is typically not taken into consideration in ocean modelling (see e.g. Jones and Toba (2001)). It is also worth noting the strong seasonal cycle (50% peak to trough) of this index *I*. During the winter, the mean wind speeds and the associated variability are much higher than during the summer in the KOE region. This is probably the reason for the strong seasonal cycle of the index *I*. Seasonal cycle of *I* has been suggested by Hanawa and Toba (1987), who have investigated meteorological buoy data south of Japan. In our study, we have confirmed their finding analyzing the numerical weather forecast products.

Furthermore, we found a systematic increase of this ratio (about 4%) in 1998, when the ECMWF operational model first introduced two-way coupling of wind-wave model and the atmospheric model. This suggests that the surface roughness ($z_0$) variations due to wind-wave effectively increased the daily wind stress; before 1998, $z_0$ depended only on friction velocity but after 1998 it also depends on the wave age (ratio of the wave phase speed to the wind speed). Indeed the wind-wave parameters also show a strong seasonal cycle (plot not shown), suggesting that the additional variation of the wind stress can come through changes of the drag coefficient due to wave age. Therefore, the turbulence in the atmospheric boundary layer is enhanced due to sea surface roughness variability induced by wind wave.

In summary, it is crucial to pay more attention to the impact of high-frequency wind forcing at both synoptic and turbulence time scales when forcing an ocean model, and the stress should not be estimated from daily mean wind. We therefore chose to use the J-OFURO product, which provides the daily mean wind stress as an average of the stresses in a time-space ellipsoid rather than deriving wind stress from mean wind vector.

## 3. Impact of QuikSCAT Wind on the Kuroshio Path

We used a Kuroshio-Oyashio model that is a version of a $\sigma$-coordinate primitive equation solver (POM Blumberg and Mellor, 1983) developed at JAMSTEC (Mitsudera *et al.*, 1997) to cover the main Kuroshio stream along the southern Japan coast, the Oyashio current in the north, and the Kuroshio extension region; the approximate domain is from 125°E to 170°E, 20°N to 52°N, configured to have a curvilinear coordinate system in which the horizontal axes follow the mean geometry of the Kuroshio stream. The horizontal resolution of the model varies between 1/6 degrees to 1/12 degrees within the model domain, and 32 sigma-levels are configured in depth. The model has successfully run in different settings, for example with various Kuroshio inflow rates. Hellerman-Rosenstein wind (Hellerman and Rosenstein, 1983), COADS heat flux (Slutz *et al.*, 1985) and the Levitus monthly climatologies (Levitus, 1982) were used for the surface boundary conditions, the initial temperature and salinity fields, and the lateral boundary restorations for the control cases.

Various sensitivity tests conducted with the model suggest that the primary control parameter in determining the Kuroshio path state is the inflow transport. In the control case, with fixed 35 Sv transport and Hellerman-Rosenstein annual mean wind forcing (HR, hereafter), the Kuroshio switches naturally between straight and meander paths. In Figs. 7 and 8, the mean transport stream functions south of the Kuroshio are presented in the left; the 10 year mean (from model year 6 to 15) during the meandering path stage and the 10 year mean (from year 16 to 25) during the straight path stage, respectively. During the meandering period the transport and the size of the SRG is much larger than during the straight path state. This is also depicted in the right-hand-side figures, which show the scatter plot of the transport stream function ($\Psi$) versus barotropic potential vorticity (Q). The maximum transport is about 90 Sv in the meandering path stage and is about 77 Sv in the straight path stage.

It is worth taking a closer look at the $\Psi$-Q diagram, to understand the mean state of the SRG. For example, a linear dependence of Q on $\Psi$ suggests that the potential

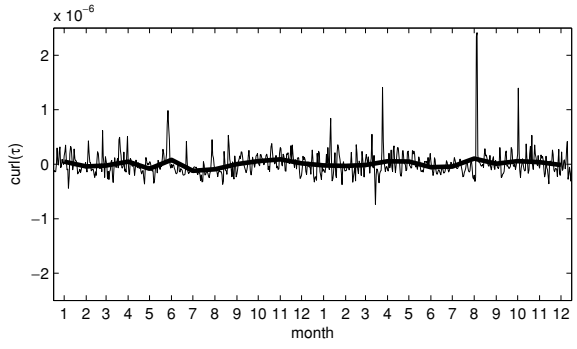


Fig. 5. Time series of wind stress curl at 135°E 30°N from January 2000 to December 2001. Thin line is the daily mean wind stress curl and thick line is the monthly mean.

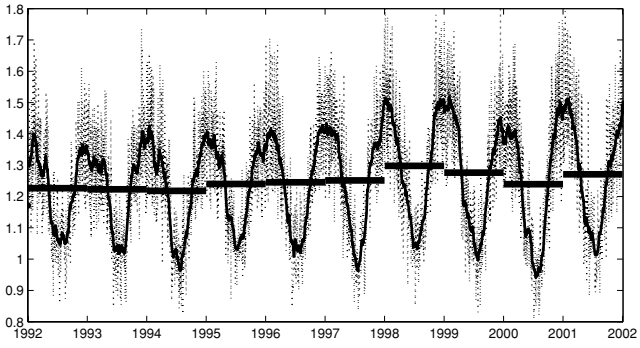

Fig. 6. Ratio of the daily mean wind stress to the wind stress derived from daily mean wind speed. Solid line is a 30-day running mean and thick horizontal line is the annual mean.

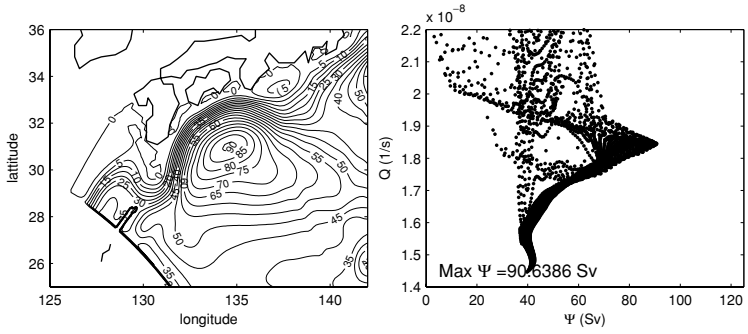


Fig. 7. Left: 10-year mean transport stream function; right: scatter plot of the transport stream function ($\psi$) and barotropic potential vorticity ($Q$) for the meandering stage (year 6 to 15). Scattered points represent 10 year mean values on the model grids offshore Japan, approximately between the southern tip of the Kyushu Island and the Kii peninsula.

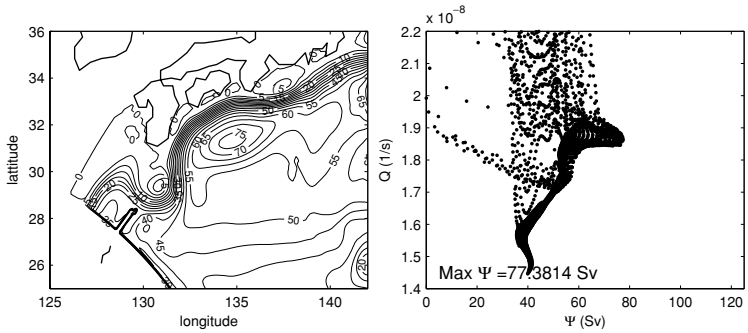


Fig. 8. Left: 10-year mean transport stream function; right: scatter plot of the transport stream function ($\psi$) and barotropic potential vorticity ($Q$) for the straight path stage (year 16 to 25).

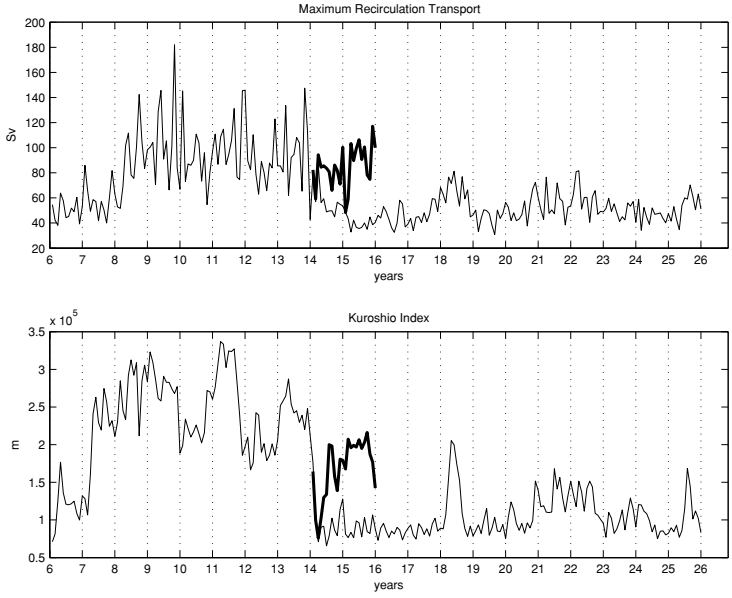


Fig. 9. Top: Time series of the Shikoku recirculation gyre strength defined as the maximum transport stream function. Bottom: Time series of the Kuroshio Index defined as the mean Kuroshio axis distance (0.7 m sea surface height isoline) between the Kii peninsula and the Boso peninsula. Thin solid line is from the control run with 35 Sv inflow and Hellerman-Rosenstein annual mean wind forcing. Thick solid line is from the perturbation run using QuikSCAT-derived daily mean wind forcing.

vorticity is advected along the transport stream line which is a characteristic of the Fofonoff type gyre; see, for example, the diagonal cluster of points in the diagram. On the other hand, in the straight path stage, there is a region where Q becomes homogenized (between 60 and 70 Sv), indicating that a weak viscosity is effectively mixing the potential vorticity within the SRG, as suggested by the extension of the Prandtl-Batchelor theorem in a rotating frame of reference (Yamagata and Matsuura, 1981; Rhines and Young, 1982). Hence, the mean state of the SRG can be considered as near inertial where the potential vorticity fluxes by eddy transport, wind forcing and dissipation are nearly in balance (Niiler, 1966; Marshall and Nurser, 1986).

Next we investigate the time evolution of the Kuroshio with particular emphasis on the transition between the meander and the straight path state. At model year 7, the averaged Kuroshio axis distance from the coast between the Kii peninsula and the Boso peninsula (Kuroshio index) increases rapidly and remains large until the end of year 13 (Fig. 9 bottom). After year 14, the Kuroshio remains straight. Plotted in the top figure is a time series of the maximum SRG transport defined in the domain that approximately covers the SRG (shown in Fig. 10). The maximum transport of the SRG appears closely correlated (0.69) with the amplitude of the Kuroshio meander, suggesting that the strength of the SRG is a critical parameter in determining the Kuroshio path state.

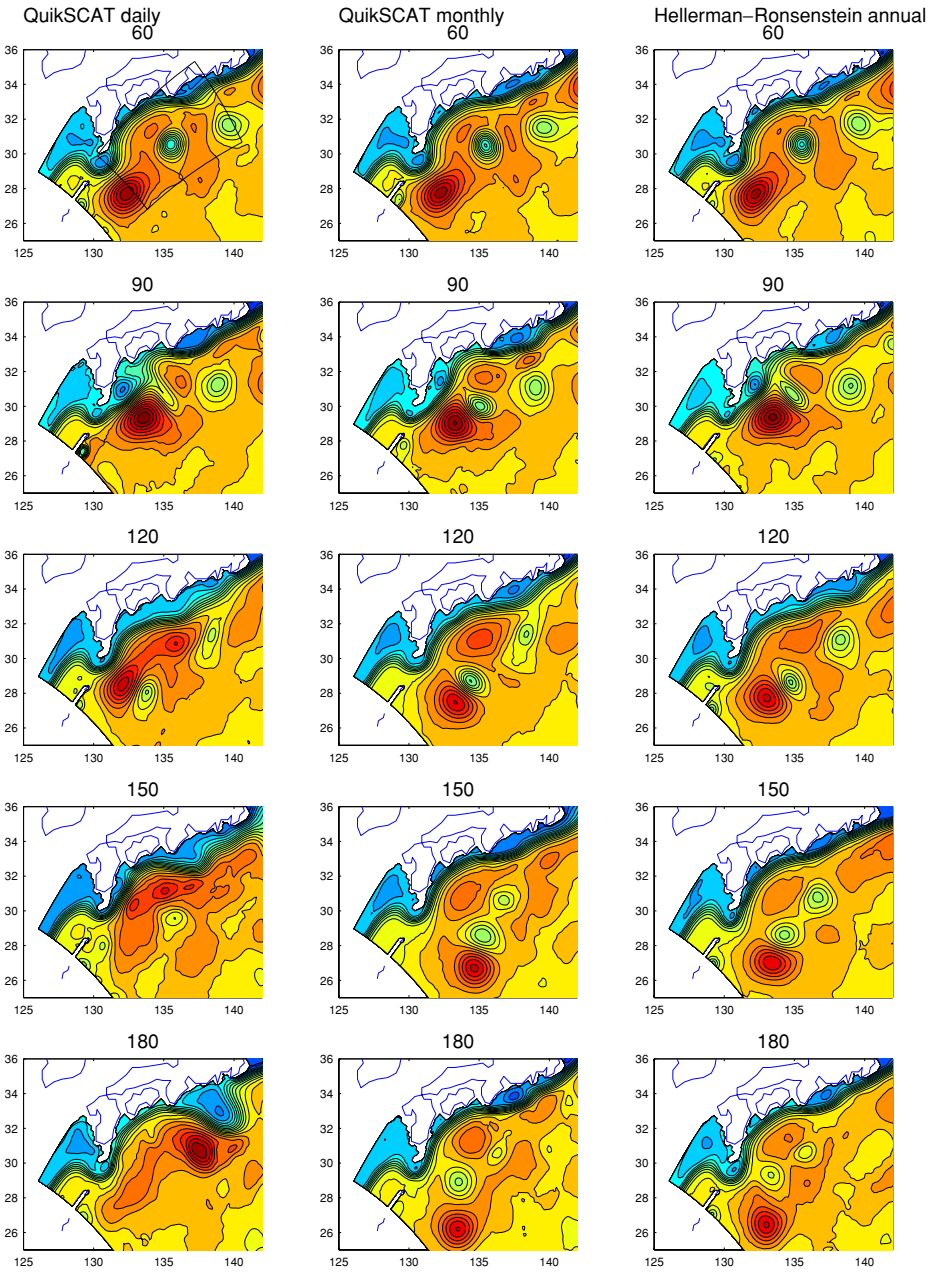


Fig. 10. Daily mean SSH snapshots showing the evolution of the Kuroshio path states. Right column: Day 60 to 180 of year 14 of the control case with Hellerman-Rosenstein annual mean wind forcing. Center column: wind forcing was switched to QuikSCAT-derived monthly mean forcing from year 14. Left column: wind forcing was switched to daily mean QuikSCAT wind forcing from year 14. Area indicated in the upper leftmost figure is the defined SRG domain to estimate the SRG strength.

Plotted in the thick solid lines of Fig. 9 is the case of QuikSCAT wind forcing. At year 14 of the control case (35 Sv inflow), the wind forcing was switched from annual mean HR wind stress to daily mean QuikSCAT-derived wind stress (J-OFURO). While the Kuroshio remains straight after year 15 in the former case, it meanders in year 16 with daily mean wind forcing (thick solid line, bottom figure). Accompanying the transition from straight to meander, the maximum transport of the SRG increases (top figure) as if the strength of the SRG is a surrogate for the Kuroshio path state. What makes the maximum transport of the SRG a parameter control the

path state, and what caused the difference in the SRG strength in the two cases? The answer is the anticyclonic eddy within the SRG. As suggested by Mitsudera *et al.* (2001), both satellite observation and in-situ observation suggest that a strong anticyclonic eddy exists within the SRG and interacts with the Kuroshio. The anticyclonic eddy was quite strong with maximum surface velocity around 70 cm $s^{-1}$ and the horizontal scale around 300 km or so and rotates within the SRG in a clockwise direction, causing the meander amplitude to oscillate over a few months period. When such a strong anticyclonic eddy exists within the SRG, the maximum transport becomes quite large.

Now let us look into the temporal evolution of the sea surface height field from our numerical simulation. Figure 10 shows the sequence of the sea surface height (SSH) snapshots at 30-day intervals from day 60 of year 14 for the QuikSCAT daily mean run (first column), QuikSCAT monthly mean run (second column), and Hellerman-Rosenstein annual mean run (third column). Taking a glance at the case of the QuikSCAT daily mean forcing, we notice that the transition from straight to meander path occurs when the anticyclonic eddy is advected along the Kuroshio, from day 60 to 180, just as suggested by previous studies on the interaction of the Kuroshio and the anticyclonic eddy (Mitsudera *et al.*, 2001; Ebuchi and Hanawa, 2003; Waseda *et al.*, 2003). On the other hand, with Hellerman-Rosenstein annual mean wind forcing, the same eddy detaches from the Kuroshio (at day 120) and migrates southward; as a result, the Kuroshio continues to take a straight path (day 180). The migration of the eddy out of the SRG will coincide with the reduction of the magnitude of the maximum SRG transport (Fig. 9 top). Thus, in this case the SRG strength decreases because the anticyclonic eddy migrated away from the SRG. Plotted in the center column of Fig. 10 is the sequence of SSH in the case of QuikSCAT monthly mean run. The sequence closely resembles that of the annual mean forcing where the eddy migrates south (right column), suggesting that the relevant time scale of the fluctuation of the wind field to perturb the motion of the anticyclonic eddy was less than a month.

In a previous study, Waseda *et al.* (2002) have shown that a small change in the thermocline displacement of the initialized eddy resulted in its distinct evolution. With relatively large thermocline displacement the eddy migrated toward the west, but with smaller thermocline displacement the eddy migrated toward the south, advected by a barotropic eddy pair that grew in time. The study demonstrated that the eddy in this region is in the frontal geostrophic regime where the dynamical balance is achieved between nonlinearity and dispersion. With the addition of the baroclinicity arising from some kind of an instability, it makes the evolution of an eddy highly sensitive to small difference in its scale. It is then conceivable that a perturbation from the high-frequency wind may cause a large difference in the evolution of the anticyclonic eddy as a result of nonlinearity.

Table 1. Summary of QuikSCAT perturbation runs.

| | East daily | East monthly |
|---|---|---|
| West daily | meander | meander |
| West monthly | straight | straight |

We can now conclude that the difference in the Kuroshio path evolution between monthly (or annual) mean wind forcing and daily wind forcing comes from the difference in the motion of the strong anticyclonic eddy in the SRG which was perturbed by "local" wind. To prove that, we have conducted the following additional experiments: QuikSCAT daily mean forcing west of the Izu ridge, QuikSCAT monthly mean forcing east of the Izu ridge; and QuikSCAT monthly forcing west of the Izu ridge, QuikSCAT daily mean forcing east of the Izu ridge. The results are summarized in Table 1. These results consistently support the conclusion that it is the local (west of the Izu ridge) high-frequency (less than a month) wind that is responsible for the transition of the Kuroshio path to a meandering state. This proves that the local high-frequency wind perturbed the anticyclonic eddy and caused it to move distinctly from the monthly (or annual) mean wind forcing cases.

## 4. Summary and Conclusion

Advances in satellite scatterometry, numerical weather prediction, and data assimilation enabled high-wavenumber and high-frequency wind and stress products to be made available globally at 6 hourly and daily intervals. Recently, using scatterometer-derived wind products, Xie *et al.* (2001) have shown that the blocking of the trade wind by high mountains in the Hawaiian islands generates anomalous local wind-stress curl, triggering the generation of an eastward flowing ocean current west of the islands. While such study successfully demonstrates the significance of a high-wavenumber wind stress to the ocean circulation, few studies have been made of the impact of the temporal change of the wind stress on the currents. Will the high-frequency wind impact the strong Kuroshio current in the western north Pacific where the temporal variability of the wind stress is quite high as a result of a series of atmospheric lows and highs passing by Japan?

To answer this question we first analyzed and compared various wind stress products and then studied the impact of high-frequency, high-wavenumber wind stress to the Kuroshio path south of Japan by numerical experi-

ment. The former study suggested that the daily mean wind stress derived from daily mean wind speed can significantly underestimate the wind stress because of the large subdiurnal variation of the stress. However, not all the satellite-derived products deliver the mean of the wind stress vector. Instead of deriving the mean stress using bulk formula from the mean wind speed, J-OFURO averages the stress vector at full spatio-temporal resolution. With the best product available to us, we have proceeded further to conduct a sensitivity experiment with the regional Kuroshio model.

The results of the numerical simulation showed that the Kuroshio path evolution differed between the monthly (or annual) mean and the daily mean wind forcing cases because of the distinct trajectory of the strong anticyclonic eddy within the SRG. In the latter case, the high-frequency wind forcing perturbed the anticyclonic eddy and the eddy trajectory switched from southward to northward migration. Because the anticyclonic eddy is highly nonlinear, the high-frequency wind forcing provides sufficient perturbation to alter the motion of the eddy. Such geostrophic perturbation can come from other sources as well; the Kuroshio inflow fluctuation and eddies inpinging on the SRG from upstream and downstream Kuroshio (Kawabe, 1995; Endoh and Hibiya, 2000, 2001; Akitomo and Kurogi, 2001). The result suggests that it is the strong anticyclonic eddy within the SRG that controls the Kuroshio path variations in agreement with the previous studies by Mitsudera *et al*. (2001), Ebuchi and Hanawa (2000), Waseda *et al*. (2003). When the strong anticyclonic eddy is in the SRG it is likely that the Kuroshio is in a meandering state. Indeed, our study showed that the correlation of the SRG strength (maximum transport) and the Kuroshio path state is quite high; further observational evidence should be provided in the future.

Finally, during the winter, our analysis showed that the mean wind stress can be 50% larger than the stress derived from the mean wind speed due to subdiurnal variation. In the KOE region, the effective increase of the drag coefficient was between 0 and 50% with a strong seasonal cycle. Since most of the satellite-derived products only provide wind vectors, using them to estimate the wind stress may significantly underestimate their magnitude. To remedy that, one can use the index $I$ estimated in Section 2 to adjust the wind stress derived from the daily mean wind speed,

$$\tau_{daily} = \rho I C_D U_{daily}^2. \qquad (3)$$

Here, $I$ incorporates both the temporal variation of the wind speed and the drag coefficient. As shown in Fig. 6, index $I$ has a strong seasonal cycle which is not usually taken into consideration when bulk formula is used.

**Acknowledgements**

The first author thank Prof. Hanawa of the Tohoku University who has kindly introduced us with his original work on the long-term mean air-sea momentum transfers. The authors thank Diane Henderson of the SOEST library for her careful editorial review. The two reviewers who made constructive comments have helped improve the quality of the paper. Part of the research was funded by the MEXT initiative, Research Revolution 2002, through its program "Development of 4-D data assimilation system and construction of data base for climate research" of JAMSTEC (lead-PI T. Awaji). The research was conducted at the International Pacific Research Center of the University of Hawaii, which is partially funded by the Frontier Research System for Global Change. IPRC publication number 302, SOEST publication number 6503.

**References**

Akitomo, K. and M. Kurogi (2001): Path transition of the Kuroshio due to mesoscale eddies: A two-layer, wind driven experiment. *J. Oceanogr*., **57**, 735–741.

Akitomo, K., T. Awaji and N. Imasato (1991): Kuroshio path variation south of Japan 1. Barotropic inflow-outflow model. *J. Geophys. Res*., **96**(C2), 2549–2560.

Akitomo, K., S. Masuda and T. Awaji (1997): Kuroshio path variation south of Japan: Stability of the paths in a multiple equilibrium regime. *J. Oceanogr*., **53**, 129–142.

Blumberg, A. F. and G. L. Mellor (1983): Diagnostic and prognostic numerical circulation studies of the South Atlantic Bight. *J. Geophys. Res*., **88**, 4579–4592.

Bonekamp, H., G. J. Komen, A. Sterl, P. A. E. M. Janssen, P. K. Taylor and M. J. Yelland (2002): Statistical comparisons of observed and ECMWF modeled open ocean surface drag. *J. Phys. Oceanogr*., **32**, 1010–1027.

Chao, S. Y. (1984): Bimodality of the Kuroshio. *J. Phys. Oceanogr*., **14**, 92–103.

Ebuchi, N. and K. Hanawa (2000): Mesoscale eddies observed by TOLEX-ADCP and TOPEX/POSEIDON altimeter in the Kuroshio recirculation region south of Japan. *J. Oceanogr*., **56**, 43–57.

Ebuchi, N. and K. Hanawa (2003): Influences of mesoscale eddies on variations of the Kuroshio path south of Japan. *J. Oceanogr*., **59**(1), 25–36.

Endoh, T. and T. Hibiya (2000): Numerical study of the generation and propagation of trigger meanders of the Kuroshio south of Japan. *J. Oceanogr*., **56**(4), 409–418.

Endoh, T. and T. Hibiya (2001): Numerical simulation of the transient response of the Kuroshio leading to the large meander formation south of Japan. *J. Geophys. Res*., **106**(C11), 26,833–26,850.

Hanawa, K. and Y. Toba (1987): Critical examination of estimation method of long-term mean air-sea heat and momentum transfers. *Ocean-AirInteractions*, **1**, 79–93.

Hellerman, S. and M. Rosenstein (1983): Normal monthly wind stress over the world ocean with error estimates. *J. Phys. Oceanogr*., **13**, 1093–1104.

Hurlburt, H. E., A. J. Wallcraft, W. J. Schmitz, Jr., P. J. Hogan and E. J. Metzgar (1996): Dynamics of the Kuroshio/Oyashio current system using eddy-resolving models of the North Pacific Ocean. *J. Geophys. Res.*, **101**(C1), 941–976.

Imawaki, S., K. Ichikawa, S. Aoki, Y. Fukuda, S. Ito, H. Kawamura, M. Kubota, T. Kuragano, K. Matsumoto, T. Nagai, A. Sengoku and H. Yoritaka (2001a): Mass, heat and salt transports in the western North Pacific. *AVISO Altimetry NEWSLETTER*, **8**, 62–64.

Imawaki, S., H. Uchida, H. Ichikawa, M. Fukasawa, S. Umatani and the ASUKA Group (2001b): Satellite altimeter monitoring the Kuroshio transport south of Japan. *Geophys. Res. Lett.*, **28**(1), 17–20.

Jones, I. S. F. and Y. Toba (2001): *Wind Stress over the Ocean*. Cambridge, U.K., 307 pp.

Kagimoto, T. and T. Yamagata (1996): Seasonal transport variations of the Kuroshio: An OGCM simulation. *J. Phys. Oceanogr.*, **27**(3), 403–418.

Kawabe, M. (1985): Sea level variations at the Izu Islands and typical stable paths of the Kuroshio. *J. Oceanogr. Soc. Japan*, **41**, 307–326.

Kawabe, M. (1995): Variations of current path, velocity, and volume transport of the Kuroshio in relation with the large meander. *J. Phys. Oceanogr.*, **25**, 3103–3117.

Kubota, M., N. Iwasaka, S. Kizu, M. Konda and K. Kutsuwada (2002): Japanese ocean flux data sets with use of remote sensing observations (J-OFURO). *J. Oceanogr.*, **58**(1), 213–225.

Kutsuwada, K. (1998): Impact of wind/wind-stress field in the North Pacific constructed by ADEOS/NSCAT data. *J. Oceanogr.*, **54**(2), 301–314.

Large, W. G. and S. Pond (1981): Open ocean momentum flux measurements in moderate to strong winds. *J. Phys. Oceanogr.*, **11**, 324–336.

Levitus, S. (1982): *Climatological Atlas of the World Ocean*. U.S. Dept. of Commerce and NOAA, 173 pp.

Marshall, J. and G. Nurser (1986): Steady, free circulation in a stratified quasi-geostrophic ocean. *J. Phys. Oceanogr.*, **16**, 1799–1813.

Masuda, A. (1982): An interpretation of the bimodal character of the stable Kuroshio path. *Deep-Sea Res.*, **29**, 471–484.

Mitsudera, H., Y. Yoshikawa, B. Taguchi and H. Nakamura (1997): High-resolution Kuroshio/Oyashio system model: Preliminary results. *JAMSTECR*, **36**, 147–155 (in Japanese with English abstract).

Mitsudera, H., T. Waseda, Y. Yoshikawa and B. Taguchi (2001): Anticyclonic eddies and Kuroshio meander formation. *Geophys. Res. Lett.*, **28**(10), 2025–2028.

Niiler, P. P. (1966): On the theory of wind-driven ocean circulation. *Deep-Sea Res.*, **13**, 597–606.

Nishimura, T. (1998): The coherent structure inside the oceanic turbulence around Japan-islands-chain. Technical Report, Science University of Tokyo, Noda-City 278-8510, Japan.

Qiu, B. and W. Miao (2000): Kuroshio path variation south of Japan: bimodality as a self-sustained internal oscillation. *J. Phys. Oceanogr.*, **30**, 2124–2137.

Rhines, P. B. and W. R. Young (1982): Homogenization of potential vorticity in planetary gyres. *J. Fluid Mech.*, **122**, 347–367.

Slutz, R. J., S. J. Lubker, J. D. Hiscox, S. D. Woodruff, R. L. Jenne, D. H. Joseph, P. M. Steurer and J. D. Elms (1985): Comprehensive ocean-atmosphere data set; release 1. Technical Report 268, NOAA Environmental Research Laboratories, Climate Research Program, Bolder, Colo., U.S.A.

Waseda, T., H. Mitsudera, B. Taguchi and Y. Yoshikawa (2002): On the eddy-Kuroshio interaction: Evolution of the mesoscale eddy. *J. Geophys. Res.*, 10.1029/2000JC000756:01.

Waseda, T., H. Mitsudera, B. Taguchi and Y. Yoshikawa (2003): On the eddy-Kuroshio interaction: Meander formation processes. *J. Geophys. Res.*, 10.1029/2002JC001583:3220.

White, W. B. and J. P. McCreary (1976): On the formation of the Kuroshio meander and its relationship to the large-scale ocean circulation. *Deep-Sea Res.*, **23**, 33–47.

Xie, S.-P., W. T. Liu, Q. Liu and M. Nonaka (2001): Far-reaching effects of the Hawaiian Islands on the Pacific ocean-atmosphere. *Science*, **292**, 2057–2060.

Yamagata, T. and T. Matsuura (1981): A generalization of Prandtl-Batchelor theorem for planetary fluid flows in a closed geostrophic contour. *J. Meteor. Soc. Japan*, **59**(5), 615–619.

Yasuda, I. and J. H. Yoon (1987): Dynamics of the Kuroshio large meander: Two-layer model. *J. Phys. Oceanogr.*, **17**, 66–81.

Yasuda, I., J. H. Yoon and N. Suginohara (1985): Dynamics of the Kuroshio large meander—barotropic model. *J. Oceanogr. Soc. Japan*, **41**, 259–273.

Yelland, M. and P. Taylor (1996): Wind stress measurements from the open ocean. *J. Phys. Oceanogr.*, **26**, 541–558.